Pilz, M., Cotton, F. (2019): Does the One-Dimensional Assumption Hold for Site Response Analysis? A Study of Seismic Site Responses and Implication for Ground Motion Assessment Using KiK-Net Strong-Motion Data. - *Earthquake Spectra*, *35*, 2, pp. 883—905.

DOI: http://doi.org/10.1193/050718EQS113M

Does the One-Dimensional Assumption Hold for Site Response Analysis? A Study of Seismic Site Responses and Implication for Ground Motion Assessment Using KiK-Net Strong-Motion Data

Marco Pilz[a] **and Fabrice Cotton**[a),b)]

The one-dimensional (1-D) approach is still the dominant method to incorporate site effects in engineering applications. To bridge the 1-D to multidimensional site response analysis, we develop quantitative criteria and a reproducible method to identify KiK-net sites with significant deviations from 1-D behavior. We found that 158 out of 354 show two-dimensional (2-D) and three-dimensional (3-D) effects, extending the resonance toward shorter periods at which 2-D or 3-D site effects exceed those of the classic 1-D configurations and imposing an additional amplification to that caused by the impedance contrast alone. Such 2-D and 3-D effects go along with a large within-station ground motion variability. Remarkably, these effects are found to be more pronounced for small impedance contrasts. While it is hardly possible to identify common features in ground motion behavior for stations with similar topography typologies, it is not over-conservative to apply a safety factor to account for 2-D and 3-D site effects in ground motion modeling. [DOI: 10.1193/050718EQS113M]

INTRODUCTION

Over the last 30 years, investigations of seismic site effects in areas with particular local geological and morphological features, such as alluvial basins and isolated hills, have been the main topic of many studies in earthquake engineering and engineering seismology. In this context, reliable and accurate evaluation of site effects in urban areas represents an important target in the framework of seismic risk mitigation strategies. At a given site, if the seismic record is known for outcropping (i.e., reference) bedrock, the filtering effects produced by the presence of soft sediments can be assessed from the knowledge of a horizontally layered geotechnical model of the soil column. The one-dimensional (1-D) amplification models are widely applied in ground response analysis and ground motion modeling (e.g., Rathje et al. 2010, Rodriguez-Marek et al. 2014, Haji-Soltani and Pezeshk 2017). If site-specific data is not available or only a limited amount of information is accessible, several seismic codes [e.g., Eurocode 8 (EC8) by the European Committee for Standardization (CEN) 2004,

[a] Helmholtz Centre Potsdam, GFZ German Research Centre for Geosciences, Telegrafenberg, 14473 Potsdam, Germany; Email: pilz@gfz-potsdam.de (M. P.)
[b] Universität Potsdam, Institut für Erd- und Umweltwissenschaften, Karl-Liebknecht-Str. 24-25, 14476 Potsdam, Germany

the Italian Building Code (NTC 2008), and International Code Council (ICC) 2006, 2009] account for site effects using response spectra with modified spectral shape based on soil categories defined according to a 1-D proxy: V_{S30} (the equivalent time-averaged shear-wave velocity from the surface to a depth of 30 m).

In reality, however, seismic site response is influenced not only by the local (i.e., 1-D) site conditions but also by the three-dimensional (3-D) environment, such as bedrock slope, geometry of the soft soil layers, and topographical irregularities. One of the main pieces of empirical evidence of 3-D amplification effects comes both from the concentration of structural damage near topographic irregularities (such as a hill, a ridge, a canyon, a cliff, or a slope) as observed during past and recent earthquakes (e.g., Wyllie and Bolt 1986, Çelebi 1987) and instrumental data (e.g., Davis and West 1973), clearly indicating that surficial morphology and topography can affect the propagation of seismic motion, which, in turn, can lead to significantly modified levels of ground shaking because of scattering, diffraction, or trapping of waves.

In sedimentary valleys and basins with complex two-dimensional (2-D) and 3-D geometries, deviations from 1-D site response can be related to two phenomena. In narrow and deep valleys, interference of surface waves with vertically propagating waves might give rise to the evolution of 2-D resonance patterns (e.g., Kagami et al. 1982, Bard and Bouchon 1985). In rather shallow valleys for which 1-D resonance effects are prevalent, the interaction of the earthquake wavefield with particular structural geometries and velocity contrasts at the basin boundaries might give rise to the generation of surface waves at the basin edge (Aki and Larner 1970, Boore et al. 1971, Toriumi 1975, Bard and Bouchon 1980a, 1980b).

A quantitative description of the limits of the 1-D assumption and corresponding predictions of the influence of 2-D and 3-D effects, however, remains a difficult task. While a large number of numerical studies have focused on simulations in idealized 2-D basins with well-known shapes of the sediment-bedrock interface and idealized topographies (e.g., Hisada and Yamamoto 1996, Makra et al. 2012, Hasal and Iyisan 2014, Zhu and Thambiratnam 2016, Riga et al. 2016, 2018, Zhu et al. 2018), only a small number (e.g., Thompson et al. 2012, Laurendeau et al. 2018) have tried to evaluate the validity of the 1-D assumption and identify the different levels of complexity of site response that should be accounted for. Thompson et al. (2012) analyzed 104 arrays in Japan that have recorded surface acceleration higher than 0.3 g and concluded that 16 of these sites resemble the 1-D site response. This study evidenced the occurrence of 2-D and 3-D effects and the fact that the effects of soil heterogeneity can be confounded with soil nonlinearity. In contrast, Laurendeau et al. (2018), applying similar criteria, concluded that around two-thirds of their selection met the 1-D properties. However, the relatively small number of 1-D sites detected by Thompson et al. (2012) raises the question of to which degree 2-D and 3-D effects can be quantified and integrated easily in engineering ground-shaking predictions (Rassem et al. 1997, Pitilakis et al. 2001, Choi et al. 2005, Ansal 2006, Riga et al. 2016).

The aim of this paper, then, is to experimentally test the validity of the 1-D assumption and also investigate the ability to identify 2-D and 3-D site effects for Kiban Kyoshin network (KiK-net) sites and quantify their impact on the amplitude and variability of ground motions. After a short presentation of the data set, we identify KiK-net sites with reliable velocity profiles and 1-D site responses. We then investigate the ability to detect and take into account

2-D and 3-D effects using site-condition proxies (topographic slope, soil thickness, distance from the basin edge). We finally quantify the differences of ground motions observed on 1-D and 2-D or 3-D sites, allowing some preliminary recommendations for the introduction of multidimensional effects in the seismic design of structures and for ground motion modeling.

DATA SET

In this study, earthquake recordings from the KiK-net strong-motion network are analyzed. The KiK-net is currently composed of 689 sites, which are each equipped with a pair of surface and downhole sensors. Most of the downhole stations are located between 100 and 200 m. The data set further includes a collection of *P*- and *S*-wave velocity profiles, which were obtained from downhole logging in boreholes set up for the installation of buried sensors. However, most KiK- net stations are located on rock or thin sedimentary sites (Okada et al. 2004), with around two-thirds of the sites exhibiting V_{S30} values smaller than 550 m/s.

At all KiK-net sites, we collected accelerograms recorded between 2008 and 2017 with a Japan Meteorological Agency (JMA) magnitude between 3.5 and 7.7 taken from the Full Range Seismograph Network of Japan (F-net) catalog and a hypocentral depth less than 35 km and an epicentral distance below 300 km. Dawood et al. (2016) concluded that the hypocentral location and magnitude from the F-net catalog can be considered more reliable than the KiK-net data. In addition to these restrictions, we chose only earthquakes with at least three usable recordings for which the peak ground acceleration at the surface was less than 0.1 g to keep the analysis in the linear range. Soil nonlinearity is expected to have only a minor effect on the occurrence of 2-D or 3-D effects, mainly because it will affect the top layer where small values of effective overburden stress are present (Gelagoti et al. 2012). From the whole data set, 17,646 recordings pass the criteria. Their distribution is shown in Figure 1.

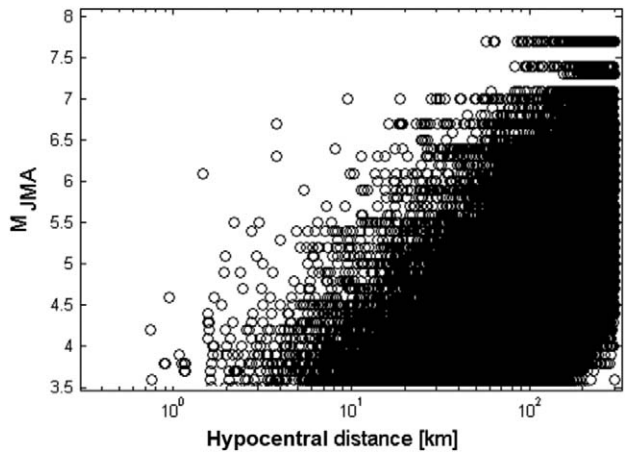

Figure 1. Distributions of magnitude (M_{JMA}) against hypocentral distance for all recordings used in this study.

CALCULCATION OF THE EMPIRICAL AMPLIFICATION FUNCTIONS

Because interferences of up- and down-going waves may lead to destructive interferences at depth, we refrain from directly calculating surface-to-downhole spectral ratios for each network site. In contrast, empirical amplification functions are calculated following the inversion procedure presented by Edwards et al. (2013). For each recorded event, i, we apply a baseline correction of the acceleration time histories. The P-wave and S-wave arrivals and the signal end (end of coda waves) are automatically picked up. The algorithm used for automatic selection is based on the calculation of the ratio of the long-term average (LTA) over the short-term average (STA). It continuously calculates the average values of the absolute amplitude of the waveform signal in two consecutive moving time windows. To identify the local events, we chose an LTA of 5 s, an STA of 1 s, and threshold of 0.5 (Trnkoczy 2002). If no S-wave arrivals were available, a P-to-S ratio of 1.73 was used. The analyzed window comprises the 5%–95% energy integral around the S-wave and the coda. After integration of the accelerograms, the corresponding Fourier velocity spectrum Ω_{ij} observed at station j is given by the following:

$$\Omega_{ij}(f,r) = 2\pi f\, E_i(f, M_{0i}, f_{ci})\, B_{ij}(f, t^*_{ij})\, S_{ij}(r, r_{0\ldots n-1}, \lambda_{1\ldots n})\, T_j(f, A_j, \kappa_j) \tag{1}$$

in which f is the frequency, r is the hypocentral distance, $E_i(f, M_{0i}, f_{ci})$ is the source model, $B_{ij}(f, t^*_{ij})$ is the intrinsic attenuation along the ray path with attenuation parameter $t*$ (following Anderson and Hough 1984), $S_{ij}(r, r_{0\ldots n-1}, \lambda_{1\ldots n})$ is the frequency-independent amplitude decay with distance (geometrical spreading), and $T_j(f, A_j, \kappa_j)$ is the site response function at station j. The source spectrum E_i is considered to be a Brune (1970, 1971) ω^2-spectrum with an event-specific corner frequency, f_c, and a long-period spectral plateau defined by the seismic moment M_{0i}. Oth et al. (2010) showed that for KiK-net data, the source spectra can be well explained using the ω^2-model. The geometric spreading function, S_{ij}, is described as a decay function with a constant frequency-independent exponential decay in the form $r^{-\lambda}$. An initial spherical decay (i.e., $\lambda = 1.0$) is followed by attenuation slightly lower than spherical with $\lambda = 0.9$ for $r > 150$ km (Kawase 2006).

The local site response is given by:

$$T_j(f, A_j, \kappa_j) = A_j a_j(f) e^{-\pi f \kappa_j} \tag{2}$$

in which A_j is the average site response relative to a given regional reference (as described below), $a_j(f)$ is the normalized frequency-dependent elastic site response function, and κ_j is the site-dependent local attenuation parameter.

However, a strong trade-off does exist between the moment and the average amplification. To decouple the site effect from the magnitude determination, M_{JMA} values determined by the JMA taken from the F-net catalog are fixed when available. No significant differences between M_{JMA} and M_w were found for shallow events (Katsumata 1996), which are mostly encountered in this study.

A nonlinear, two-stage regression is used to separate the different contributions of Equation 1 for obtaining $T_j(f, A_j, \kappa_j)$. We first determine the combined path and site attenuation $(t^*_{ij} + \kappa_j)$ at each site, the event-common source corner frequency, f_c, and a spectral

amplitude parameter termed the signal moment for each spectrum. A regional attenuation model is not used to predetermine $t^*_{ij} + \kappa_j$ because this requires simultaneous inversion of the full data set (rather than the event-by-event application) and might bias the results because of model simplification. The misfit of the spectral model to the data is minimized in the log-log space using the $L2$ least-squares norm. Using the resulting minimum misfit model, the residuals are then assumed to be an estimate of the normalized frequency-dependent elastic component of the site function $a_j(f)$. Consequently, by correcting for the geometric decay function S_{ij}, the frequency-independent component of the modeled spectra, the signal moments, can be split into a single seismic moment M_0 and a site response term A_j relative to a common reference. Based on Poggi et al. (2013), we adopt a gradient-like functional form for the Japanese reference profile. The profile is characterized by a steep increase in velocity from around 1,100 m/s at the surface to almost 3,000 m/s at a depth of 300 m. The V_{S30} of the Japanese reference is around 1,350 m/s.

RELIABILITY OF KIK-NET VELOCITY PROFILES

Because downhole logging has been shown to not be fully reliable for some KiK-net sites (Kawase and Matsuo 2004, Wu et al. 2017), we need to define quantitative criteria to distinguish sites with properly resolved velocity profiles from others, so that further analyses are not biased by unreliable velocity profiles. For downhole sensors located close to or below the deepest impedance contrast, the reliability of the provided velocity profiles can then be based on the comparison of the fundamental resonance frequencies directly estimated from the empirical amplification function and by indirect modeling of the *SH* wave transfer function using the given velocity profiles and a correction for the reference rock. The 2-D and 3-D effects such as basin-edge–induced surface waves do not affect the fundamental frequency (e.g., Cornou et al. 2003, Kumar and Narayan 2008). To compute the theoretical *SH* wave transfer function for vertically propagating waves, we follow the Knopoff layer-matrix formulation (Knopoff 1964). Because no information about density is available from the logging profiles, we rely on proposed dependencies between density and *P*-wave velocity, $\rho = 0.31 v_P^{0.25}$ (Gardner et al. 1974). The frequency-independent site-specific *S*-wave quality factors, Q_S, were determined from the empirical relationships between Q_S and V_S (Campbell 2009) and range from 1.5 to 156 with a median of 9.3.

We define a sufficient match between the empirical amplification function and the modeled transfer function if the ratio between the measured and the calculated fundamental resonance frequency is between 0.5 and 2 and if the correlation coefficients between the flanks of the two functions around the fundamental resonance frequency are higher than 0.5. Although such assumptions do not rule out sites for which amplification occurs over a broad frequency band because of strong lateral variations at depth, this criterion could be fulfilled for 287 sites only. When this criterion was not satisfied, we followed the strategy of Cadet et al. (2012) and applied the same matching condition that has been used for the fundamental resonance frequency as well as for the first higher mode of the theoretical *SH* transfer function. In addition to the 287 sites described above, this criterion was fulfilled for another 67 sites. Because the position and the amplitude of the fundamental resonance frequency is mainly controlled by the deepest impedance contrast, the second condition was established because of the non-negligible likelihood that the fundamental peak in the empirical amplification function is rejected because of a relatively low amplitude with respect to its standard deviation.

However, for the modeled transfer function, the first peak usually has significantly higher values because of pure interferences in case of vertical incidence and is thus less likely to be rejected.

From the whole data set of 689 sites, 354 sites (51%) were found to have reliable velocity profiles and were kept for further analysis. This quantitative selection of KiK-net sites is somewhere in the middle of the number of sites analyzed in previous works (Cadet et al. 2012, Poggi et al. 2012, Thompson et al. 2012). The selection spans a range of sites with average *S*-wave velocity over the first 30 m between 120 m/s and 1,260 m/s. It covers 15 sites with EC8 soil class A ($V_{S30} > 800\,\mathrm{m/s}$), 172 sites for soil class B ($360\,\mathrm{m/s} < V_{S30} < 800\,\mathrm{m/s}$), 144 sites for soil class C ($180\,\mathrm{m/s} < V_{S30} < 360\,\mathrm{m/s}$), and 13 sites for soil class D ($V_{S30} < 180\,\mathrm{m/s}$). The variability of the fundamental frequency is also well represented, spanning a broad range between 0.7 Hz and 15 Hz.

DETECTION AND PARAMETERIZATION OF 2-D AND 3-D EFFECTS IN THE FOURIER DOMAIN

The quantitative detection of 2-D and 3-D effects is based on the comparison of the empirical amplification function with the theoretical transfer function over the entire frequency band (Chávez-Garcia and Faccioli 2000, Cornou and Bard 2003, Thompson et al. 2012). The empirical amplification function integrates all geometrical effects, whereas non–1-D wave propagation phenomena such as edge-generated surface waves and topographic or focusing effects cannot be reproduced by 1-D transfer functions. Because the theoretical transfer function is based on upwardly propagating plain body waves, it allows higher mode resonances to be seen in a high-frequency range. As the amplification functions have been corrected for the Japanese reference rock and are therefore directly comparable between all sites, deviations from observed amplification functions (i.e., the corresponding aggravation factors) can be related to the occurrence of 2-D and 3-D effects.

Figure 2 presents a comparison of measured and modeled amplification functions. Though for sites HDKH01 and YMGH107, the theoretical transfer function matches the empirical data well both in terms of resonance frequencies and amplitudes, for sites HRSH07 and IBUH06, significant differences in amplitude and shape can be found for frequencies higher than the site's fundamental frequency. However, for sites HRSH07 and IBUH06, an increasing number of peaks is observed in the high-frequency range. Such wiggles are due to the dispersive nature of basin-edge–induced Rayleigh waves and have already been observed in numerical studies (Narayan and Kumar 2014). Similar deviations also occur if amplification effects occur over broad frequency ranges because of topographic effects.

Similar to Thompson et al. (2012) we establish a quantitative criterion for the match of the two amplification functions. To this regard, we calculate Spearman's rank-order correlation coefficient r (Spearman 1904) on logarithmically spaced samples to ensure a constant number of points at low and high frequencies. The calculation is carried out in a frequency range between the site's fundamental frequency and 25 Hz. As described by Thompson et al. (2012), the amplification functions at frequencies below the fundamental one usually show a gradual monotonic increase, which does not affect r. Spearman's correlation coefficient is a rank-based version of Pearson's correlation coefficient (Pearson 1895) and, therefore,

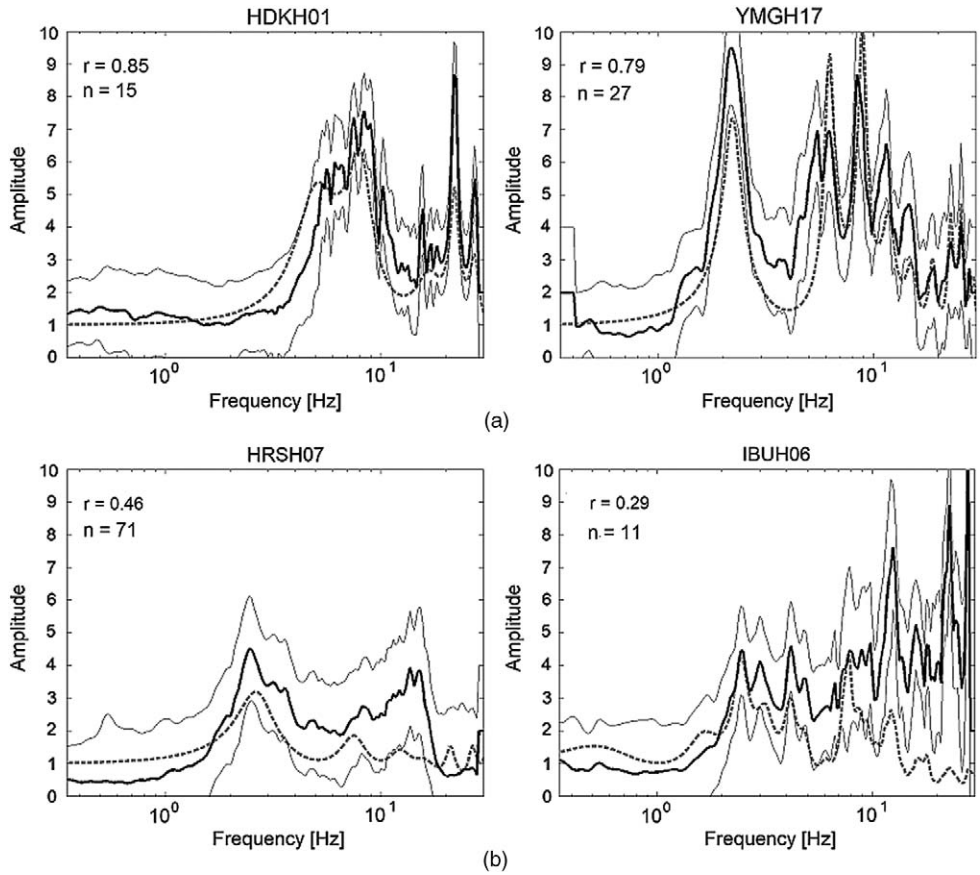

Figure 2. Theoretical 1-D *SH* transfer function for four KiK-net sites (gray dotted lines). The black lines represent the average measured empirical amplification function plus/minus one standard deviation. (a) HDKH01 and YMGH07 are representative sites for which the 1-D transfer function accurately predicts the empirical transfer function. (b) For sites HRSH07 and IBUH06, a significant mismatch between both amplification functions for frequencies higher than the fundamental frequency is found. *r* represents Spearman's rank-order correlation coefficient. *n* indicates the number of records used to derive the empirical amplification functions.

is superior because Pearson's correlation requires the two curves to be linearly related, which might introduce false correlations or mask existing ones (Devlin et al. 1975). On the contrary, the Spearman coefficient does not care about the exact amplitude values but about comparing the shape of the two curves. We consider potential trade-offs in the spectral inversion between elastic amplification and anelastic attenuation that may lead to incorrect amplification levels at high frequencies.

Based on visual inspection between the measured and modeled transfer functions and estimates of the confidence interval for Spearman's correlation coefficient for a sample data set of 354 sites (Caruso and Cliff 1997), we define a threshold of $r > 0.6$ to classify

sites as 1-D. The classification is objectively assessed based on the comparison of the shape of the empirical amplification function for frequencies higher than f_0. Of the 354 remaining sites in our database with reliable velocity profiles, 196 are classified as strictly 1-D, whereas 158 sites (45%) do not fulfil these criteria and are classified as sites exhibiting 2-D and 3-D effects. As can be seen in Figure 3, there is a similar number of stations in each bin for small values of r, whereas the number starts to increase for $r > 0.5$. Changing the threshold of $r = 0.6$ for classifying stations as 1-D and 2-D or 3-D will slightly modify the number of sites in each class, but it will not affect the results of this study substantially.

Besides numerical studies focusing on idealized 2-D models, only few attempts have been made for applying classification schemes to wider areas and real-world data sets (e.g., Burjánek et al. 2014, Maufroy et al. 2014, Rai et al. 2016a, 2016b). While the aforementioned studies were focusing only on the occurrence of topographic amplification effects, Thompson et al. (2012) concluded that only 16 out of 100 sites fulfil the criteria for 1-D site conditions (low interevent variability and good fit to the 1-D transfer function). Laurendeau et al. (2018) applied similar selection criteria to a limited subset of KiK-net sites, concluding that around two-thirds of their selection meet the 1-D criteria. Our study only considers one of these two criteria (good fit to the 1-D transfer function) and only motions in the linear domain, which might explain why our results are different from these two studies. The results, however, in agreement with Thompson et al. (2012), confirm the limits of the 1-D assumption and the need to take into account 2-D and 3-D effects.

While none of the aforementioned studies have explored the utility of Digital Elevation Models (DEMs) and their derived topographic attributes, we try to incorporate digital terrain

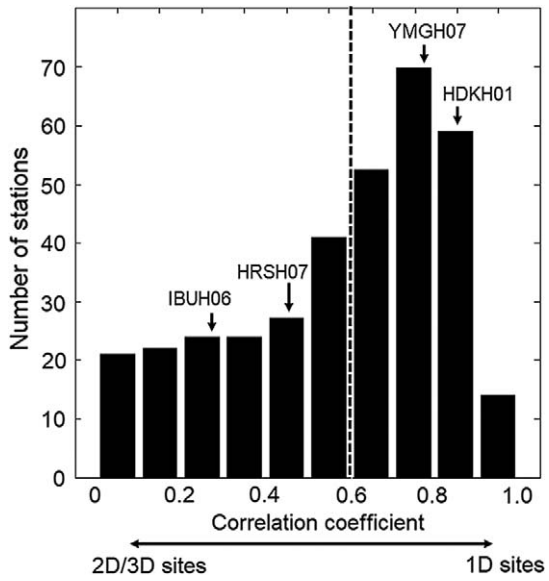

Figure 3. Classification scheme for 1-D and 2-D or 3-D sites according to Spearman's correlation coefficient. The arrows indicate r for the four representative sites shown in Figure 1.

representations. For our study, we use a 1 arc s or approximately 30 m resolution DEM data. The corresponding elevation data based on the Advanced Spaceborne Thermal Emission and Reflection Radiometer (ASTER) Global DEM (GDEM) version 2 data can be downloaded from the ASTER GDEM web site (NASA Jet Propulsion Laboratory 2011). We first project the DEM to a native Universal Transverse Mercator (UTM) coordinate system. For each grid cell of the raster, we calculate the elevation and its mean first spatial derivative, the slope, from a grid around the central cell. A positive slope value indicates that the central cell has a lower elevation than the mean elevation in the neighborhood, while negative slope values represent higher elevations for the central cell than the mean elevation in the neighborhood. We further determine the shortest distance of each recording site from the edge of the valley or basin. Using an automatic procedure, we first define the minimum bounding geometry of the watershed polygon (Figure 4) and determine the dimension of the basin where a strongly concave break in the slope occurs (Bull 1977). The shortest path from this break to the network site represents the distance to the basin edge. Such automatic procedure could be applied for 92 sites only.

While 2-D and 3-D effects are not limited to a specific level of elevation, the occurrence of such effects is mainly limited to slightly positive slope values (Figure 5a). This seems to indicate that sites with high fundamental frequencies are only affected by 2-D and 3-D effects if they are close to the edge of the basin, whereas for larger distances, 2-D and 3-D effects also occur for sites with low fundamental frequencies. Correspondingly, for shallow valleys and basins with corresponding near-surface impedance contrasts, 2-D and 3-D effects only affect sites close to the basin edge. Figure 5b further suggests that 2-D and 3-D site effects are more important for large velocity contrasts, and they hardly occur for small values of H_{800} (the depth beyond which V_S exceeds 800 m/s). This mainly involves V_{S30} values smaller than ~500 m/s (subsoil classes C and lower class B of EC8), while it appears that 2-D and 3-D effects have only a minor influence for higher values of V_{S30} and corresponding smaller velocity contrasts that are less efficient for the generation and trapping of surface waves.

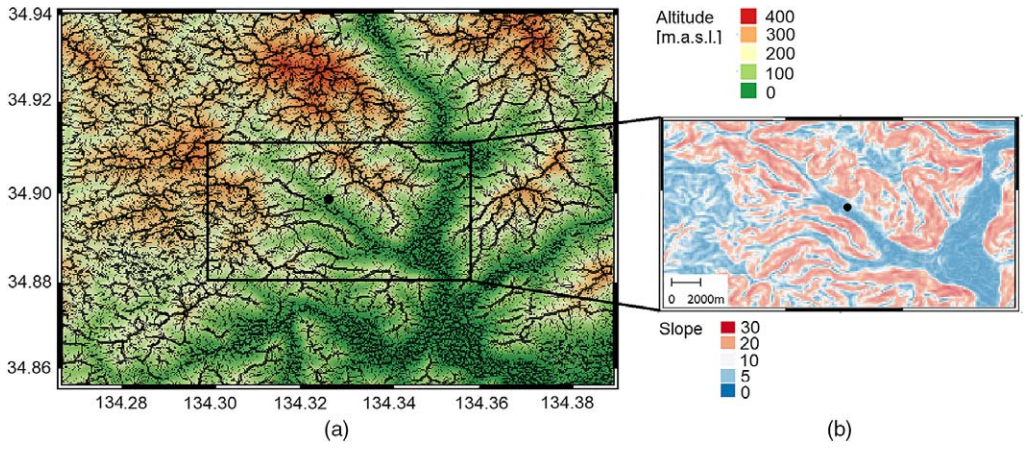

Figure 4. (a) Digital elevation model with the black lines representing watershed ridges and (b) topographic slope. The black dot represents the location of seismic station HYGH05.

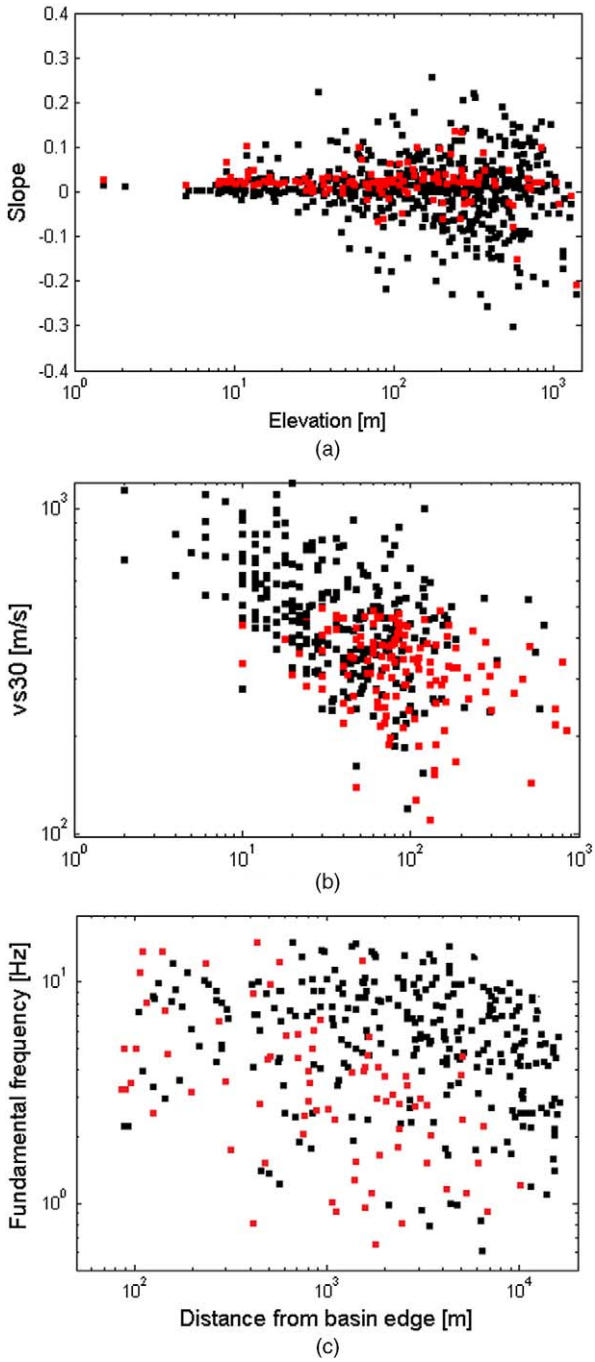

Figure 5. (a) Topographic slope against absolute elevation. (b) Vs_{30} against H_{800}. (c) Fundamental resonance frequency against distance from basin edge. Here, only 92 sites are presented. For the remaining sites, no distance from basin edge could be determined. Black dots indicate 1-D sites, while red dots indicate 2-D and 3-D sites. See text for further discussion.

1-D AND 2-D OR 3-D AMPLIFICATION FACTORS IN THE RESPONSE SPECTRA DOMAIN

From an engineering point of view, response spectra represent a more appropriate way for describing the level of ground motion. The response spectra S_a for a given oscillator period T is the maximum acceleration of a single-degree-of-freedom system with damping ratio ξ to a base excitation. In the following, we assume $\xi = 5\%$. From the measured surface ground motion, we calculate observed response spectra $S_a^o(T)$ using a set of geometric means of the two horizontal components rotated to all possible orthogonal rotation angles (Boore et al. 2006) and compare these values with the predicted response spectra $S_a^p(T)$. The latter are calculated from the predicted ground motion at the surface. These ground motion values can be obtained by an inverse Fourier transform of the predicted amplitude spectrum at the surface. The latter amplitude spectra can be obtained by a convolution of the amplitude spectrum of the downhole record with the *SH* 1-D transfer function with respect to the Japanese reference rock profile as defined above. From the ground motion values at the surface, the associated $S_a^p(T)$ is obtained. Corresponding S_a residuals are calculated as the common logarithm of the $S_a^o(T)/S_a^p(T)$ ratio; i.e., negative residuals represent an overprediction, whereas positive values indicate underpredictions.

Figure 6 compares the observed $S_a^o(T)$ and the predicted $S_a^p(T)$ response spectra. While for 1-D sites, the mean is centered around 0, for 2-D and 3-D sites, the peaks of the residuals attain values larger than 0.15 (which means an amplification of 40%) in the considered period range (0.06–1 s). Correspondingly, the mean also indicates a significant underprediction for periods smaller than 1 s.

GROUND MOTION PREDICTION EQUATION RESIDUALS FROM 1-D AND 2-D OR 3-D SITES

As a general trend, 2-D and 3-D effects widen the period range of amplification toward shorter periods at which 2-D or 3-D site effects exceed those of the classical 1-D

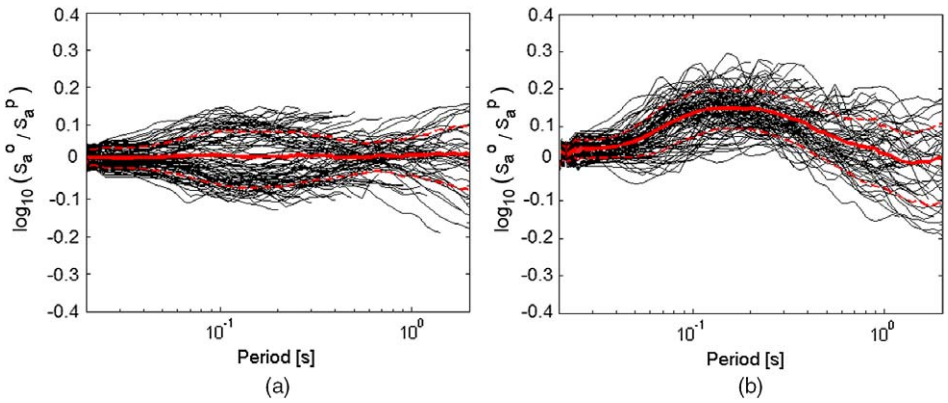

Figure 6. Residuals of response spectra for 5% damping represented as logarithm of observed $S_a^o(T)$ divided by predicted $S_a^p(T)$ for (a) 196 sites that are 1-D and (b) 158 sites at which 2-D or 3-D effects occur. The red lines represent the mean plus/minus one standard deviation.

configuration. This indicates that 2-D and 3-D effects do contribute significantly to the surface ground motion in the short period range, imposing a large amplification in addition to that caused by impedance contrast alone. However, these effects diminish for periods larger than the site's fundamental period. On the contrary, for very short periods ($T < 0.05$ s), the differences between the two curves disappear drastically because of attenuation. Such anelastic attenuation affects 2-D and 3-D site responses to a larger extent than 1-D response. This is natural, as the larger 3-D peaks result from the contributions of laterally propagating waves, which travel longer paths than vertically propagating body waves in the 1-D model.

The analysis is based on a mixed-effects regression approach (as in Abrahamson and Youngs 1992), which makes it possible to identify statistically significant random effects for all relevant parameters. Following Rodriguez-Marek et al. (2013) and using the notation of Al Atik et al. (2010), we derive a ground motion prediction equation as follows:

$$\ln S_a(T) = f(M_W, R_{JB}, V_{S30}) + \delta B_e + \delta W_{es} \tag{3}$$

where $\ln S_a(T)$ is the natural logarithm of the observed spectral acceleration at a site for period T; and $f(M_W, R_{JB})$ is the median prediction from a ground motion model with a given moment magnitude, M_W, and a Joyner-Boore distance, R_{JB}. The model site response depends on V_{S30} only. δB_e is the average between-event residual of the ground motion prediction equation for a given earthquake, e, which is common at all sites with zero mean and standard deviation, τ. δW_{es} is the within-event residual, which can be partitioned into two components:

$$\delta W_{es} = \delta S2S_s + \delta WS_{es} \tag{4}$$

where $\delta S2S_s$ is the site residual, and δWS_{es} is the site- and event-corrected residual. The term $\delta S2S_s$ is the repeatable site residual that is common for each ground motion recorded at a site. Both terms can be considered as random normal variables with zero means and corresponding standard deviations of ϕ_{S2S} (site-to-site variability) and ϕ_0 (single-station event-corrected variability). As 2-D and 3-D effects are site-specific, the bias in residuals from such effects is expected to be present in the site residual.

Following a strategy similar to Kotha et al. (2018), we calibrate in the first step the magnitude-dependent distance-scaling function, and then we use the distance-corrected observations for calibrating the magnitude-scaling function. At each step, we carry out a mixed-effects regression for assessing both the δB_e and $\delta S2S_s$ random effects to ensure that the regression coefficients are not biased (further details can be found in Kotha et al. 2018). Online Appendix Figure A1 presents the event and site-corrected residuals to verify that the fixed-effect components capture the attenuation well at all magnitude, distance, and azimuth ranges. $\delta S2S_s$ results for 1-D and 2-D or 3-D sites are shown in Figure 7. $\delta S2S_s$ does not indicate the absolute site response but rather deviations from the predicted response using a V_{S30} site characterization. While the mean $\delta S2S_s$ is close to zero for 1-D sites, meaning that there are no systematic deviations of the observed amplifications from the empirically predicted median V_{S30}-based amplifications, the 2-D and 3-D effects bring the $\delta S2S_s$ further away from zero for periods longer than 0.1 s. Averaged over all sites, this

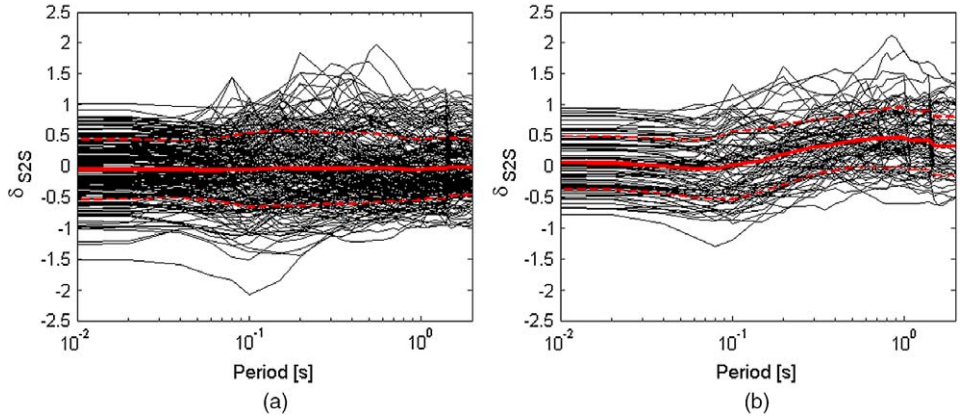

Figure 7. Site residuals $\delta S2S_s$ from Equation 4 for (a) 1-D sites and (b) sites with 2-D or 3-D effects. The red lines represent the mean plus/minus one standard deviation.

indicates an underprediction of ground motion amplification in the high-period range, with a maximum underprediction around $T = 1$ s.

Because Figure 5 has indicated that only a limited number of parameters might be used to assess 2-D and 3-D effects, the trends of $\delta S2S_s$ with varying bins of V_{S30} and f_0 are shown in Figure 8. For increasing levels of V_{S30}, the amplitude of the $\delta S2S_s$ decreases. This is most likely due to the fact that basin-edge–induced surface waves become less prominent for decreasing impedance contrasts (Narayan 2012). For all f_0 bins, $\delta S2S_s$ starts to increase for periods longer than 0.1 s, while the peak of the individual $\delta S2S_s$ is found in a period range around or slightly higher than the site's fundamental period. The effects of increasing $\delta S2S_s$ become even more prominent for sites with rather low fundamental resonance frequencies (i.e., rather thick sedimentary covers), while none of these effects can be observed for 1-D sites.

Figure 9 plots the site-to-site and single-station ground motion variability for selected periods across all 1-D and 2-D or 3-D sites. Both $\delta S2S$ and $\delta 0$ are centered; i.e., no significant difference for the mean values and for the corresponding standard deviations between 1-D and 2-D or 3-D sites can be observed. 1-D sites show the same amount of variability in their response to an earthquake as 2-D or 3-D sites, meaning that, on average, such variability is not only linked to the occurrence of 2-D or 3-D effects. 1-D sites show, however, lower values of ϕ_0 (and, correspondingly, a lower standard deviation for the mean of ϕ_0) over the entire period range; the larger variability for 2-D and 3-D sites confirms (e.g., Ktenidou et al. 2018) the sensitivity of the occurrence of 2-D and 3-D effects, with the source location influencing the azimuth, angle, and type of incident waves.

DISCUSSION

Although the scientific community is well aware of the occurrence of 2-D and 3-D effects, current ground motion models and building codes are still based on simple 1-D site proxies, ignoring complementary amplification because of 3-D structures. Our goal, however, is not a substitution of current modeling approaches, as Joyner (2000) and

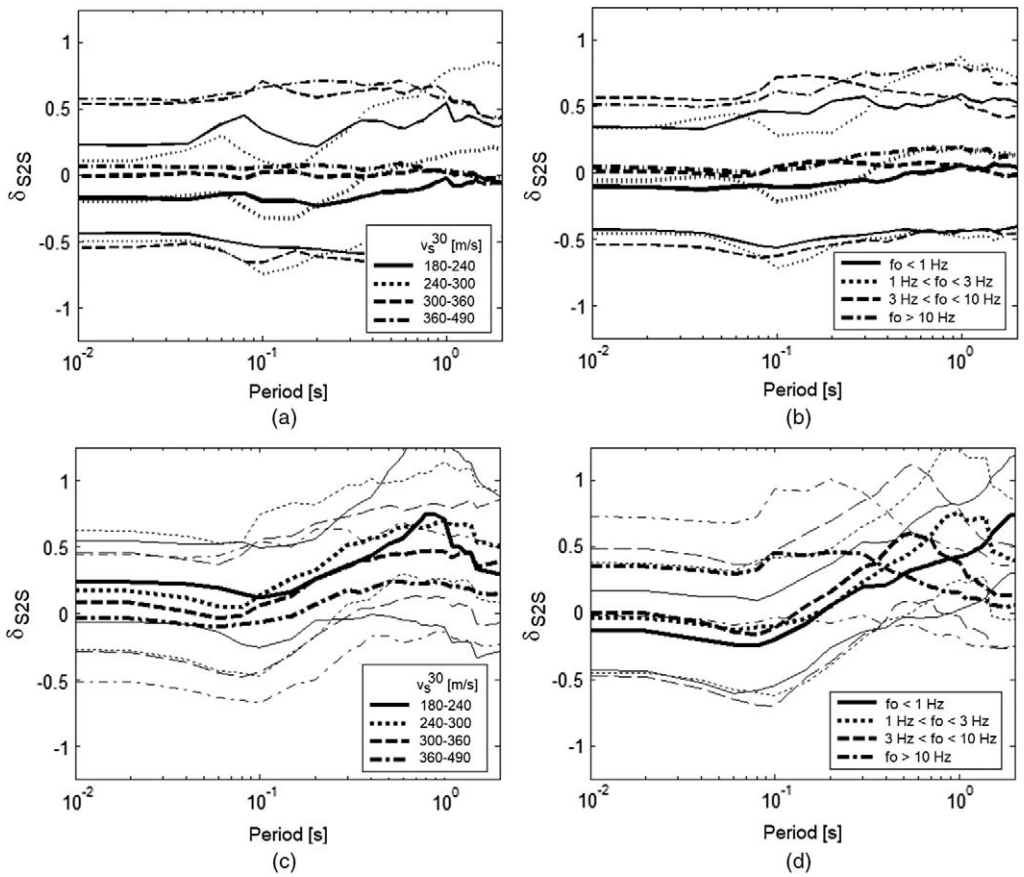

Figure 8. Variation of site residuals $\delta S2S_s$ for 1-D with (a) V_{S30} and (b) fundamental resonance frequency. Variation of site residuals $\delta S2S_s$ for 2-D or 3-D sites with (c) V_{S30} and (d) fundamental resonance frequency. The thin lines represent one standard deviation range. Sites with $V_{S30} < 180\,\mathrm{m/s}$ are not listed separately because of their limited number.

Somerville et al. (2004) already provided an empirical ground motion model accounting for basin-induced effects; we aim at evaluating the portion of sites for which 1-D site amplification models may not suffice and test proxies that may help to identify such sites. Derras et al. (2017) have already tested the performance of various site-condition proxies to minimize the variability of ground motion modeling, but they did not explicitly discuss the use of 2-D and 3-D proxies. Testing of such proxies is needed because almost half of the sites encountered in this study are classified as being exposed to 2-D or 3-D effects.

As shown by numerical studies (e.g., Narayan 2005), simple basins with homogeneous infill, in which the sedimentary cover thickens smoothly from the basin edge to the center, are characterized by an increase of basin wave amplitude with increasing distance from the basin edge and correspondingly increased 2-D or 3-D effects. Additional reverberations of surface waves between the basin edges can further contribute to an extended duration of ground

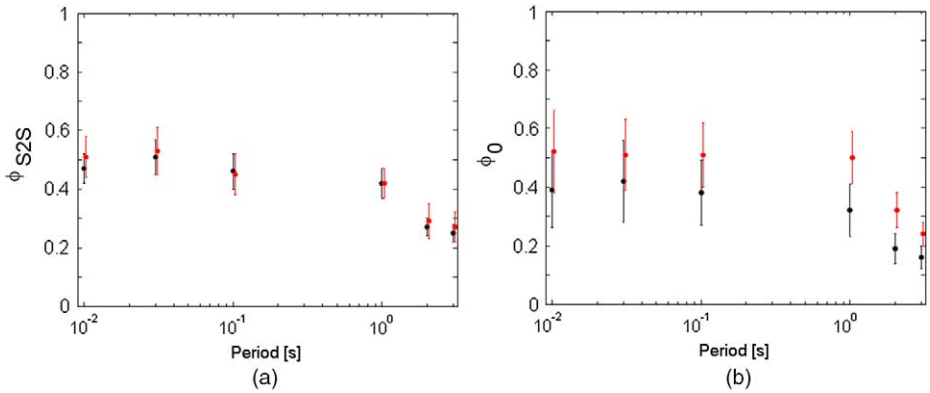

Figure 9. Standard deviation of the (a) site-to-site variability and (b) of the single-station event-corrected variability for selected periods for 1-D sites (black) and 2-D or 3-D sites (red) analyzed in this study (black cross). For each period, the dot indicates the mean and the corresponding standard deviation.

motion. Such effects are generally larger for deeper valleys with low resonance frequencies. Although, for idealized basins, the contribution of surface waves at the center of the basin is less pronounced than at the edges because of attenuation of vertically polarized basin-edge–induced waves with relatively higher frequency content of the vertical component (Narayan and Kumar 2014), Riga et al. (2016) showed that it is not the absolute distance from the basin edge but rather the relative location of the site with respect to the basin geometry.

However, for real-world sites, as employed in this study, it is difficult to determine whether the site is above the flat part of the basin or above the sloping basin edge and to have even a rough estimate of the dipping angle of the basin edge, meaning that proposing a different site classification scheme that is able to strengthen the awareness against 2-D or 3-D effects might be too complicated. In particular, averaged over all recordings of all earthquakes at KiK-net sites, the residuals of our recordings do not show a strong dependence on the distance from the basin edge and the depth of the basin (Figure 5b and 5c).

Although period-dependent aggravation factors because of 2-D and 3-D effects can be well determined for an idealized basin (Riga et al. 2016), for real-world basins, surface waves are not only induced along the direct path between the epicenter and the recording station but every point along the basin edge can induce surface waves (e.g., Pilz et al. 2018), causing difficulties to distinguish between basin-edge parallel and basin-edge normal components. All aggravation effects as shown in Figure 5 are likely to depend on the location of the individual station with respect to the topographic relief and the detailed shape of the basin edge.

Thus instead of applying complicated distance measures as indicated in Figure 4, it might be more applicable to account for the site response through the use of standardized parameters such as V_{S30} and f_0. This can also be seen in Figures 7 and 8. The use of the predominant or the fundamental site resonance frequency has been promoted recently because it is believed to be a more physical parameter than V_{S30} alone (e.g., Di Alessandro et al. 2012), and it can easily be obtained from single-station seismic noise analysis.

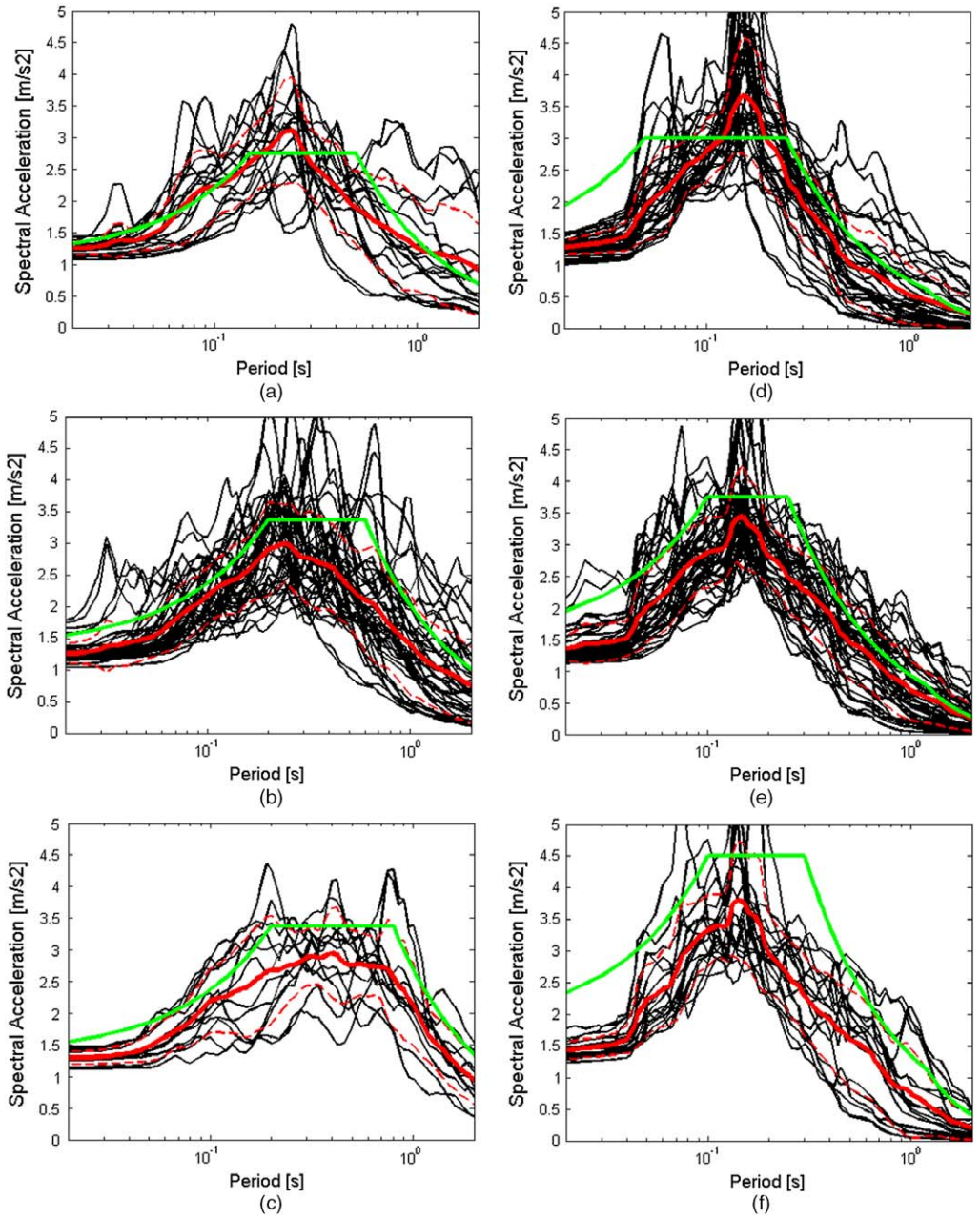

Figure 10. Elastic acceleration response spectra ($\xi = 5\%$) for 2-D and 3-D sites for Type 1 seismicity for EC8 soil classes (a) B, (b) C, and (c) D. Elastic acceleration response spectra ($\xi = 5\%$) for 2-D and 3-D sites for Type 2 seismicity for EC8 soil classes (d) B, (e) C, and (f) D. The red line corresponds to median empirical spectra plus/minus one standard deviation. The green line represents the EC8 proposed spectra.

The frequency range involved presents, however, a more fundamental issue. Although many authors observed a relation between the amplified frequency band and topography dimensions (e.g. Boore 1972, Geli et al. 1988), basin-edge–induced amplification effects become significant only for periods around and smaller than 1-D amplification (as already observed by Cornou et al. 2003 and Narayan and Singh 2006) because of the restrictions of motion of the low-velocity layers. As can be seen in Figures 2 and 9, the frequency ranges affected by basin-edge–induced effects are slightly larger than the 1-D resonance frequencies for shallow valleys and basins, and they even increase with increasing thickness-to-width ratio. As 2-D and 3-D effects are observed only for low values of V_{S30} (Figure 5b), such spectral amplification is clearly related to the impedance contrast at the basin. For high V_S ranges, neither basin-edge–induced surface waves (Narayan 2012) nor topographic effects causing a broadening of the resonance peak around and larger than the site's fundamental resonance frequency are significant (Burjanek et al. 2014).

Finally, the measured response spectra for 2-D and 3-D sites (as described in the previous section *1-D and 2-D or 3-D Amplification Factors in the Response Spectra Domain*) are compared with presently existing EC8 performance (Figure 10). For the calculation of the EC8 spectra, the general form of the equation proposed by EC8 (CEN 2004) was adopted. Although the ground motion levels specified by the earthquake provisions of current building codes such as EC8 are overlooking the influences of irregular subsurface geometries and/or surface topography, they seem to accommodate the influence of 2-D and 3-D effects well. Although our study could not identify KiK-net sites with 2-D and 3-D effects for soil class A, for soil classes B, C, and D, the spectral shapes provided by EC8 are in good agreement with the derived empirical data for both seismicity types (1 and 2) prescribed in EC8. For soil class D, the sample of data is not as rich as for the other soil classes; hence the results may not be as convincing as for remaining soil classes. For soil classes B and C, the EC8 spectra seem to be conservative enough for medium and high periods, while the lower end of the plateau could probably be slightly shifted toward lower periods; however, such minor modifications do not really justify the proposition of improved shapes for EC8 for the moment. Only for very low values of V_{S30} (soil class D) do the predicted spectra seem slightly overconservative. It should be emphasized, however, that the results represent an average over different regions.

CONCLUSIONS

We examined the combined influence of bedrock slope, topographic effects, geometry of the soft soil layers, 2-D resonances, and basin-edge–induced surface waves on earthquake ground motion. Based on statistical analysis and a quantitative comparison of the shapes of the empirical amplification function and the modeled 1-D *SH* transfer function, 45% of the 354 sites in our database of KiK-net sites with reliable velocity profiles can be classified as sites exhibiting 2-D or 3-D effects. While only a limited number of proxies might be used to assess the general occurrence of 2-D or 3-D effects for the entire data set, several previously proposed parameters, such as the dependence of the amplitude of ground motion on basin depth and distance from the basin edge, were found to not apply to the real-world data set as a whole. Given the large variability of strong-motion data, an analysis of the site residuals from the ground motion model for 2-D and 3-D sites shows that, independent of the site's fundamental period, the event's magnitude, Joyner-Boore distance, and azimuth, the site

amplification starts to increase for periods longer than 0.1 s, with a maximum $\delta S2S_s$ around or slightly larger than the site's fundamental period. The amplitude of $\delta S2S_s$ is inversly proportional to V_{S30}. This confirms that 2-D and 3-D site effects are more important for low V_{S30} and large velocity contrasts. Regarding the engineering consequences of the occurrence of 2-D and 3-D effects, only minor inconsistencies appeared when comparing the 2-D and 3-D spectra with the proposed EC8 spectrum shapes. This is not surprising, as the EC8 spectra were calibrated on empirical data and not on 1-D simulations. For sites with limited site-specific information, a generic safety factor might be applied because of the larger single-station variability for 2-D and 3-D sites. We would like to emphasize that the presented approach is not attempting to understand the physical basis of 2-D and 3-D effects (several other papers have already discussed these effects); the main goal was extracting the average consequences of 2-D and 3-D effects on ground motion modeling. Such efforts do not necessarily negate further work for obtaining better predictions by using more sophisticated physical models.

ACKNOWLEDGMENTS

We thank the National Research Institute for Earth Science and Disaster Prevention (NIED) for providing data for this analysis.

APPENDIX

Please refer to the online version of this manuscript to access the supplementary material provided in the Appendix.

REFERENCES

Abrahamson, N. A., and Youngs, R. R., 1992. A stable algorithm for regression analysis using the random effects model, *Bulletin of the Seismological Society of America* **82**, 505–510.

Aki, K., and Larner, K. L., 1970. Surface motion of a layered medium having an irregular interface due to incident plane SH waves, *Journal of Geophysical Research* **75**, 933–954.

Al Atik, L., Abrahamson, N., Bommer, J. J., Scherbaum, F., Cotton, F., and Kuehn, N., 2010. The variability of ground-motion prediction models and its components, *Seismological Research Letters* **81**, 794–801.

Anderson, J. G., and Hough, S. E., 1984. A model for the shape of the Fourier amplitude spectrum of acceleration at high frequencies, *Bulletin of the Seismological Society of America* **74**, 1969–1993.

Ansal, A., 2006. *Recent Advances in Earthquake Geotechnical Engineering and Microzonation*, Springer, Amsterdam, The Netherlands.

Bard, P. Y., and Bouchon, M., 1980a. The seismic response of sediment-filled valleys. Part 1. The case of incident SH waves, *Bulletin of the Seismological Society of America* **70**, 1263–1286.

Bard, P. Y., and Bouchon, M., 1980b. The seismic response of sediment-filled valleys. Part 2. The case of incident P and SV waves, *Bulletin of the Seismological Society of America* **70**, 1921–1941.

Bard, P. Y., and Bouchon, M., 1985. The two-dimensional resonance of sediment-filled valleys, *Bulletin of the Seismological Society of America* **75**, 519–541.

Boore, D. M., 1972. A note on the effect of simple topography on seismic SH waves, *Bulletin of the Seismological Society of America* **62**, 275–284.

Boore, D. M., Lamer, K., and Aki, K., 1971. Comparison of two independent methods for the solution of wave scattering problems: Response of sedimentary basin to vertically incident SH waves, *Journal of Geophysical Research* **76**, 558–569.

Boore, D. M., Watson-Lamprey, J., and Abrahamson, N. A., 2006. Orientation-independent measures of ground motion, *Bulletin of the seismological Society of America* **96**, 1502–1511.

Brune, J. N., 1970. Tectonic stress and the spectra of seismic shear waves from earthquakes, *Journal of Geophysical Research* **75**, 4997–5009.

Brune, J. N., 1971. Seismic sources, fault plane studies and tectonics, *Eos, Transactions American Geophysical Union* **52**, 178–187.

Bull, W. B., 1977. The alluvial-fan environment, *Progress in Physical Geography* **1**, 222–270.

Burjanek, J., Edwards, B., and Fäh, D., 2014. Empirical evidence of local seismic effects at sites with pronounced topography: A systematic approach, *Geophysical Journal International* **197**, 608–619.

Cadet, H., Bard, P. Y., and Rodriguez-Marek, A., 2012. Site effect assessment using KiK-net data, Part 1: A simple correction procedure for surface/downhole spectral ratios, *Bulletin of the Seismological Society of America* **10**, 421–448.

Campbell, K. W., 2009. Estimates of shear-wave q and k0 for unconsolidated and semi-consolidated sediments in Eastern North America, *Bulletin of the Seismological Society of America* **99**, 2365–2392.

Caruso, J. C., and Cliff, N., 1977. Empirical size, coverage, and power of confidence intervals for Spearman's rho, *Educational and Psychological Measurements* **57**, 637–654.

Çelebi, M., 1987. Topographical and geological amplifications determined from strong-motion and aftershock records of the 3 March 1985 Chile earthquake, *Bulletin of the Seismological Society of America* **77**, 1147–1167.

Chávez-García, F. J., and Faccioli, E., 2000. Complex site effects and building codes: Making the leap, *Journal of Seismology* **4**, 23–40.

Choi, Y., Stewart, J. P., and Graves, R. W., 2005. Empirical model for basin effects accounts for basin depth and source location, *Bulletin of the Seismological Society of America* **95**, 1412–1427.

Cornou, C., and Bard, P. Y., 2003. Site-to-bedrock over 1D transfer function ratio: An indicator of the proportion of edge-generated surface waves?, *Geophysical Research Letters* **30**.

Cornou, C., Bard, P. Y., and Dietrich, M., 2003. Contribution of dense array analysis to the identification and quantification of basin-edge-induced waves, Part II: Application to Grenoble basin (French Alps), *Bulletin of the Seismological Society of America* **93**, 2624–2648.

Davis, L. L., and West, L. R., 1973. Observed effects of topography on ground motion, *Bulletin of the Seismological Society of America* **63**, 283–298.

Dawood, H. M., Rodriguez-Marek, A., Bayless, J., Goulet, C., and Thompson, E., 2016. A flatfile for the KiK-net database processed using an automated protocol, *Earthquake Spectra* **32**, 1281–1302.

Derras, B., Bard, P. Y., and Cotton, F., 2017. Vs30, slope, H 800 and f0: Performance of various site-condition proxies in reducing ground-motion aleatory variability and predicting nonlinear site response, *Earth, Planets and Space* **69**.

Devlin, S. J., Gnanadesikan, R., and Kettering, J. R., 1975. Robust estimation and outlier detection with correlation coefficients, *Biometrika* **62**, 531–545.

Di Alessandro, C., Bozorgnia, Y., Abrahamson, N. A., Akkar, S., and Erdik, M., 2012. GEM-PEER global ground motion prediction equations project: An overview, in *Proceedings of the 15th World Conference on Earthquake Engineering*, 24–28 September, 2012, Lisbon, Portugal.

Edwards, B., Michel, C., Poggi, V., and Fäh, D., 2013. Determination of site amplification from regional seismicity: Application to the Swiss National Seismic Networks, *Seismological Research Letters* **84**, 611–621.

European Committee for Standardization (CEN), 2004. Eurocode 8: design of structures for earthquake resistance, Part 1: General rules, seismic actions and rules for buildings, available at https://www.phd.eng.br/wp-content/uploads/2015/02/en.1998.1.2004.pdf (last accessed October 2018).

Gardner, G. H. F., Gardner, L. W., and Gregory, A. R., 1974. Formation velocity and density: The diagnostic basics for stratigraphic traps, *Geophysics* **39**, 770–780.

Gelagoti, F., Kourkoulis, R., Anastasopoulos, I., and Gazetas, G., 2012. Nonlinear dimensional analysis of trapezoidal valleys subjected to vertically propagating SV waves, *Bulletin of the Seismological Society of America* **102**, 999–1017.

Haji-Soltani, A., and Pezeshk, S., 2017. A Comparison of different approaches to incorporate site effects into PSHA: A case study for an LNG tank, *Bulletin of the Seismological Society of America* **107**, 2927–2947.

Geli, L., Bard, P. Y., and Jullien, B., 1988. The effect of topography on earthquake ground motion: A review and new results, *Bulletin of the Seismological Society of America* **78**, 42–63.

Hasal, M. E., and Iyisan, R., 2014. A numerical study on comparison of 1D and 2D seismic responses of a basin in Turkey, *American Journal for Civil Engineering* **2**, 123–133.

Hisada, Y., and Yamamoto, S., 1996. One-, two-, and three-dimensional site effects in sediment-filled basins, in *Proceedings of the 11th World Conference on Earthquake Engineering*, 23–28 June, 1996, Acapulco, Mexico.

International Code Council, 2006. *International Building Code*, Washington, DC.

International Code Council, 2009. *International Building Code*, Washington, DC.

Joyner, W. B., 2000. Strong motion from surface waves in deep sedimentary basins, *Bulletin of the Seismological Society of America* **90**, 95–112.

Kagami, H., Duke, C. M., Liang, G. C., and Ohta, Y., 1982. Observation of 1- to 5-second microtremors and their application to earthquake engineering, Part II: Evaluation of site effect upon seismic wave amplification due to extremely deep soil deposits, *Bulletin of the Seismological Society of America* **72**, 987–998.

Katsumata, A., 1996. Comparison of magnitudes estimated by the Japan Meteorological Agency with moment magnitudes for intermediate and deep earthquakes, *Bulletin of the Seismological Society of America* **86**, 832–842.

Kawase, H., 2006. Borehole observation for site effect studies, in *Proceedings of the Third International Symposium on the Effects of Surface Geology on Seismic Motion*, 30 August–1 September, 2006, Grenoble, France.

Kawase, H., and Matsuo, H., 2004. Amplification characteristics of K-NET, KiK-net and JMA Shindokei network sites based on the spectral inversion technique, in *Proceedings of the Thirteenth World Conference in Earthquake Engineering*, 1–6 August, 2004, Vancouver, Canada.

Knopoff, L., 1964. A matrix method for elastic wave problems, *Bulletin of the Seismological Society of America* **54**, 431–438.

Kotha, S. R., Cotton, F., and Bindi, D., 2018. A new approach to site classification: mixed-effects ground motion prediction equation with spectral clustering of site amplification functions, *Soil Dynamics and Earthquake Engineering* **110**, 318–329.

Ktenidou, O. J., Roumelioti, Z., Abrahamson, N., Cotton, F., Pitilakis, K., and Hollender, F., 2018. Understanding single-station ground motion variability and uncertainty (sigma): Lessons learnt from EUROSEISTEST, *Bulletin of Earthquake Engineering* **16**, 2311–2336.

Kumar, S., and Narayan, J. P., 2008. Importance of quantification of local site effects based on wave propagation in seismic microzonation, *Journal of Earth System Science* **117**, 731–748.

Laurendeau, A., Bard, P. Y., Hollender, F., Perron, V., Foundotos, L., Ktenidou, O. J., and Hernandez, B., 2018. Derivation of consistent hard rock (1000 < VS < 3000 m/s) GMPEs from surface and down-hole recordings: Analysis of KiK-net data, *Bulletin of Earthquake Engineering* **16**, 2253–2284.

Makra, K., Gelagoti, F., Ktenidou, O. J., and Pitilakis, K., 2012. Basin effects in seismic design: efficiency of numerical tools in reproducing complex seismic wavefields, in *Proceedings of 15th World Conference on Earthquake Engineering*, 24–28 September, 2012, Lisbon, Portugal.

Maufroy, E., Cruz-Atienza, V. M., Cotton, F., and Gaffet, S., 2014. Frequency-scaled curvature as a proxy for topographic site-effect amplification and ground-motion variability, *Bulletin of the Seismological Society of America* **105**, 354–367.

Narayan, J. P., 2005. Study of basin-edge effects on the ground motion characteristics using 2.5-D modelling, *Pure and Applied Geophysics* **162**, 273–289.

Narayan, J. P., 2012. Effects of P-wave and S-wave impedance contrast on the characteristics of basin transduced Rayleigh waves, *Pure and Applied Geophysics* **169**, 693–709.

Narayan, J. P., and Kumar, R., 2014. Spatial spectral amplification of basin-transduced Rayleigh waves, *Natural Hazards* **71**, 751–765.

Narayan, J. P., and Singh, S. P., 2006. Effects of soil layering on the characteristics of basin-edge induced surface waves and differential ground motion, *Journal of Earthquake Engineering* **10**, 595–614.

NASA Jet Propulsion Laboratory, 2011. Advanced Spaceborne Thermal Emission and Reflection Radiometer Global Digital Elevation Map, Version 2, available at https://asterweb.jpl.nasa.gov/gdem.asp (last accessed 5 March 2018).

NTC, 2008. Approvazione delle nuove norme tecniche per le costruzioni, Gazzetta Ufficiale della Repubblica Italiana, available from http://www.cslp.it/cslp/index.php?option=com_docman&task=doc_download&gid=3269&Itemid=10 (last accessed March 2018) (in Italian).

Okada, Y., Kasahara, K., Hori, S., Obara, K., Sekiguchi, S., Fujiwara, H., and Yamamoto, A., 2004. Recent progress of seismic observation networks in Japan: Hi-net, F-net, K-NET and KiK-net, *Earth, Planets and Space* **56**, 15–28.

Oth, A., Bindi, D., Parolai, S., and Di Giacomo, D., 2010. Earthquake scaling characteristics and the scale-(in) dependence of seismic energy-to-moment ratio: Insights from KiK-net data in Japan, *Geophysical Research Letters* **37**.

Pearson, K., 1895. Note on regression and inheritance in the case of two parents, in *Proceedings of the Royal Society of London* **58**, 240–242.

Pilz, M., Parolai, S., Petrovic, B., Silacheva, N., Abakanov, T., Orunbaev, S., and Moldobekov, B., 2018. Basin-edge generated Rayleigh waves in the Almaty basin and corresponding consequences for ground motion amplification, *Geophysical Journal International* **213**, 301–316.

Pitilakis, K. D., Makra, K. A., and Raptakis, D. G., 2001. 2D vs 3D site effects with potential applications to seismic norms: The case of EUROSEISTEST and Thessaloniki, in *Proceedings of the 15th International Society for Soil Mechanics and Geotechnical Engineering*, 27–31 August, 2001, Istanbul, Turkey.

Poggi, V., Edwards, B., and Fäh, D., 2012. Characterizing the vertical-to-horizontal ratio of ground motion at soft-sediment sites, *Bulletin of the Seismological Society of America* **102**, 2741–2756.

Poggi, V., Edwards, B., and Fäh, D., 2013. Reference S-wave velocity profile and attenuation models for ground-motion prediction equations: Application to Japan, *Bulletin of the Seismological Society of America* **103**, 2645–2656.

Rai, M., Rodriguez-Marek, A., and Yong, A. 2016a. An empirical model to predict topographic effects in strong ground motion using California small- to medium-magnitude earthquake database, *Earthquake Spectra* **32**, 1033–1054.

Rai, M., Rodriguez-Marek, A., and Asimaki, D., 2016b. Topographic proxies from 2-D numerical analyses, *Bulletin of Earthquake Engineering* **14**, 2959–2975.

Rassem, M., Ghobarah, A., and Heidebrecht, A. C., 1997. Engineering perspective for the seismic site response of alluvial valleys, *Earthquake Engineering and Structural Dynamics* **26**, 477–493.

Rathje, E. M., Kottke, A. R., and Trent, W. L., 2010. Influence of input motion and site property variabilities on seismic site response analysis, *Journal of Geotechnical and Geoenvironmental Engineering* **136**, 607–619.

Riga, E., Makra, K., and Pitilakis, K., 2016. Aggravation factors for seismic response of sedimentary basins: A code-oriented parametric study, *Soil Dynamics and Earthquake Engineering* **91**, 116–132.

Riga, E., Makra, K., and Pitilakis, K., 2018. Investigation of the effects of sediments inhomogeneity and nonlinearity on aggravation factors for sedimentary basins, *Soil Dynamics and Earthquake Engineering* **110**, 284–299.

Rodriguez-Marek, A., Cotton, F., Abrahamson, N. A., Akkar, S., Al Atik, L., Edwards, B., Montalva, G. A., and Dawood, H. M., 2013. A model for single-station standard deviation using data from various tectonic regions, *Bulletin of the Seismological Society of America* **103**, 3149–3163.

Rodriguez-Marek, A., Rathje, E. M., Bommer, J. J., Scherbaum, F., and Stafford, P. J., 2014. Application of single-station sigma and site-response characterization in a probabilistic seismic-hazard analysis for a new nuclear site, *Bulletin of the Seismological Society of America* **104**, 1601–1619.

Somerville, P. G., Collins, N. F., Graves, R. W., and Pitarka, A., 2004. An engineering ground motion model for basin generated surface waves, in *Proceedings of the 13th World Conference on Earthquake Engineering*, 1–6 August, 2004, Vancouver, Canada.

Spearman, C., 1904. The proof and measurement of association between two things, *The American Journal of Psychology* **15**, 72–101.

Thompson, E. M., Baise, L. G., Tanaka, Y., and Kayen, R. E., 2012. A taxonomy of site response complexity, *Soil Dynamics and Earthquake Engineering* **41**, 32–43.

Trnkoczy, A., 2002. Understanding and parameter setting of STA/LTA trigger algorithm, in *IASPEI New Manual of Seismological Observatory Practice, Volume 1* (P. Bormann ed.), German Research Center for Geosciences, Potsdam, Germany.

Toriumi, I., 1975. Earthquake characteristics in plain, *Proceedings of 4th Japan Earthquake Engineering Symposium*, Japan Society of Civil Engineers, Tokyo, Japan, 129–136 (in Japanese).

Wu, H., Masaki, K., Irikura, K., and Sánchez–Sesma, F. J., 2017. Application of a simplified calculation for full-wave microtremor H/V spectral ratio based on the diffuse field approximation to identify underground velocity structures, *Earth, Planets and Space* **69**.

Wyllie, L., and Bolt, B. A., 1986. The Chile earthquake of March 3, 1985, *Earthquake Spectra* **2**, 249–513.

Zhu, C., and Thambiratnam, D., 2016. Interaction of geometry and mechanical property of trapezoidal sedimentary basins with incident SH waves, *Bulletin of Earthquake Engineering* **14**, 2977–3002.

Zhu, C., Thambiratnam, D., and Gallage, C., 2018. Statistical analysis of the additional amplification in deep basins relative to the 1D approach, *Soil Dynamics and Earthquake Engineering* **104**, 296–306.

(Received 7 May 2018; Accepted 2 November 2018)